Korean J. Chem. Eng., 40(3), 512-518 (2023)
DOI: 10.1007/s11814-022-1333-7

pISSN: 0256-1115
eISSN: 1975-7220

Investigation of reduced lithium titanate spinel as insertion host for rechargeable batteries

Minji Jeong[*,,‡], Min Jin Kim[*,‡], Subin Na[*], Seulki Han[*], Eunmi Jo[*], Seung-Ho Yu[**], Taeeun Yim[***,†], and Si Hyoung Oh[*,****,†]**

*Energy Storage Research Center, Korea Institute of Science and Technology, 5, Hwarang-ro 14-gil, Seongbuk-gu, Seoul 02792, Korea
**Department of Chemical and Biological Engineering, Korea University, 145, Anam-ro, Seongbuk-gu, Seoul 02841, Korea
***Department of Chemistry, Research Institute of Basic Sciences, College of Natural Science, Incheon National University, 119 Academy-ro, Yeonsu-gu, Incheon 22012, Korea
****Division of Energy & Environment Technology, Korea University of Science and Technology, Seoul 02792, Korea
(*Received 16 August 2022 • Revised 24 October 2022 • Accepted 6 November 2022*)

Abstract−Rechargeable batteries based on reversible zinc electrodeposition in mildly acidic electrolytes have recently gained popularity, primarily because of their cost-benefit and high theoretical energy density achievable. However, issues associated with dendrite growth and the corrosion of zinc metal anodes still remain major technical roadblocks that must be overcome to ensure battery safety. Here we propose, for the first time, reduced lithium titanate (LTO) as a viable alternative anode that is capable of reversible ion intercalation at ~0.20 V vs. Zn/Zn^{2+}. Reduced LTO was prepared via simple thermochemical reduction at a mild temperature using sodium borohydride. This led to a significant reduction in the crystallite size and a drastic enhancement in the electrical conductivity, resulting in a distinct enhancement in the zinc insertion kinetics in the aqueous electrolytes, delivering a fair discharge capacity of 100 mAh g^{-1}. Structural and morphological studies confirmed that reduced LTO served as a zero-strain host for ionic intercalation. This study offers an interesting approach for developing novel intercalation hosts for rechargeable batteries based on abundant multivalent metal cations.

Keywords: Lithium Titanate, Intercalation Host, Thermochemical Reduction, Electrical Conductivity, Rechargeable Zinc Battery

INTRODUCTION

The ever-growing global market for electric vehicles (EV) and mid-/large-scale energy storage systems (ESS) for power plants with intermittent renewable energy sources (*e.g.*, solar or wind power) demands rechargeable batteries based on new chemistry, featuring more economic viability and enhanced safety compared to conventional Li-ion batteries (LIBs). Rechargeable batteries based on multivalent cations (*e.g.*, Zn^{2+}, Mg^{2+}, Al^{3+}) are emerging alternatives in these markets owing to the high abundance of these cations in the earth's crust, their chemical stability under ambient environment, as well as their environmental-benignity [1-5]. Among the aforementioned metals, zinc is an attractive anode material for rechargeable batteries because it not only has a high gravimetric and volumetric capacity (820 mAh g^{-1} and 5,854 mAh L^{-1}, respectively), but its electrodeposition in acidic aqueous electrolytes is highly reversible [6-8]. Furthermore, zinc is a sustainable resource because it can be readily recycled from waste batteries on an industrial scale via simple electrowinning [9]. Combined with an adequate cathode material, such as MnO_2, an energy density of up to 400 Wh kg^{-1} can be achieved, which is almost comparable to that of LIBs.

However, the benefits of using metallic zinc as a sustainable and high-capacity anode material in aqueous electrolytes are offset by several formidable technological challenges associated with dendrite growth and hydrogen evolution at the anode [8,10-12]. The mossy and dendritic growth of zinc deposits is considered as a potential threat to battery safety, and has been frequently reported in common electrolytes for zinc-ion batteries under mildly acidic conditions. Furthermore, the low material density of the porous dendrites and the loss of electrical contact caused by the formation of 'dead zinc' may lead to substantial degradation in the energy density and the performance. Another notable issue is the intrinsic chemical instability of zinc metal in the aqueous electrolytes, which causes corrosion and subsequent hydrogen evolution [8,10-12]. A substantial amount of active Zn may be lost due to incessant corrosion of the Zn anode during the long storage period before its actual usage. Furthermore, subsequent hydrogen evolution may lead to a significant pressure increase inside the battery container, thereby undermining battery safety. Efforts have been made to tackle these issues, including placing a protective layer on the surface of Zn to minimize the direct contact with the electrolyte [13,14] or adding various corrosion inhibitors to the electrolytes [15,16].

An intriguing alternative is the use of an insertion compound

†To whom correspondence should be addressed.
E-mail: yte0102@inu.ac.kr, sho74@kist.re.kr
‡These authors contributed equally to this work.

as an anode material that is capable of reversible intercalation of multivalent cations and is not susceptible to corrosion. Some organic and inorganic materials with relatively low electrode potentials have been proposed as plausible anode candidates, such as the Mo_6S_8 Chevrel phase [17-19], quinones [20], and polyimides [21]. The intercalation of multivalent cations into a solid host is a non-trivial undertaking [1-5]. This process generally involves a large activation barrier, which leads to slow reaction kinetics compared with the insertion of monovalent ions. The large energy barrier arises from difficulties in charge redistribution within the local structure upon insertion of multivalent ions, which are reportedly not as effective as monovalent Li^+ or Na^+ because of the doubly increased electrostatic interactions. In Mo_6S_8, the diffusion of multivalent cations is greatly facilitated by Mo_6 octahedral clusters, which enable charge sharing between a group of Mo atoms in the Mo_6 octahedron [22]. The insertion of Mg^{2+} into polyimides is known to involve the enolization of imide monomers, which facilitates charge delocalization within the aromatic moieties [21]. The insertion of a coordinated complex into a layer-expanded material was also proposed recently, but this process is accompanied by large volume expansion and requires a substantial amount of initial loading of the electrolyte in the cell [23,24]. In summary, for the efficient insertion of multivalent cations, the host material should have an appropriate geometric and electronic structure for facilitating fast charge redistribution.

In recent decades, lithium titanate spinel ($Li_4Ti_5O_{12}$, LTO) has been intensively investigated as a 'zero-strain' anode material for Li-ion batteries [25-27]. The large three-dimensional tunnel structure composed of TiO_6 and LiO_6 octahedra enables virtually no lattice expansion/shrinkage upon Li^+ insertion/extraction, although the process proceeds via a distinct two-phase reaction. The wide three-dimensional tunnels in LTO can act as favorable hosts, even for the multivalent cation insertion. This possibility was previously explored, saying that LTO can store Mg^{2+} ions via a complicated charge storage mechanism involving the formation of the $Li_7Ti_5O_{12}$ phase and Li^+ extraction, while Mg^{2+} was inserted into the structure [28-30]. The performance of LTO was further enhanced when nanoscale particles were used, and the electrical conductivity was increased by aliovalent doping [31]. In this study, reduced LTO was prepared via simple thermochemical reaction with $NaBH_4$ and was evaluated for the first time as a viable insertion host for anode materials, delivering a discharge capacity of ~100 mAh g^{-1} at C/20 with a suitable electrode potential of 0.20 V *vs.* the zinc electrode. The results suggest that enhanced electrical conductivity and crystallite size reduction play critical factors for the effective intercalation of ions into the spinel framework of the lithium titanate host.

EXPERIMENTAL

1. Material Preparation

For the synthesis of pristine LTO, stoichiometric amounts of Li_2CO_3 and TiO_2 (anatase) were ball milled (Mini-Mill Pulverisette 23, Fritsch) in ethanol for 2 h and dried in an oven at 80 °C for 2 h. The mixture was ground with a mortar and pestle, subjected to heat treatment at 800 °C for 5 h in air at a heating rate of 5 °C min^{-1}. For the synthesis of reduced LTO, as-prepared LTO (500 mg) and $NaBH_4$ (49.8 mg) were ground thoroughly using a mortar and pestle. The mixture was then heated at 400 °C for 1 h under flowing argon at a heating rate of 10 °C min^{-1}. The resulting dark-blue powder was washed with deionized water, filtered, and dried in an oven at 80 °C to obtain r-LTO.

2. Electrochemical Measurements for Li^+ Intercalation

To construct the electrode for the Li-ion batteries, a slurry was prepared by mixing the active materials (LTO or r-LTO), super P, and PVdF binder in a mass ratio of 8 : 1 : 1 in *N*-methyl-2-pyrrolidone (NMP) using a ball mill (Mini-Mill PULVERISETTE 23). Then, the slurry was cast onto an Al foil. The electrode was then dried overnight at 80 °C in a vacuum oven. Electrochemical measurements were carried out using 2032-type coin cells composed of the as-prepared cathode, Li foil anode, and polyethylene (PE) separator, with 1.0 M $LiPF_6$ in ethylene carbonate (EC)/dimethyl carbonate (DEC) (1 : 1 v/v) electrolyte. The cells were galvanostatically cycled between 1.0 V and 3.0 V at a scan rate of C/2 using a MACCOR cycler (1C=175 mA g^{-1}).

3. Electrochemical Measurements for Zn^{2+} Intercalation

For construction of the electrode for the zinc-ion batteries, a slurry was prepared by mixing the active materials (LTO or r-LTO), super P, and PVdF binder in a mass ratio of 6 : 2 : 2 in NMP using a ball mill, which was cast onto a stainless-steel foil. The electrode was then dried overnight at 80 °C in a vacuum oven. Electrochemical measurements were carried out using 2032-type coin cells composed of the as-prepared cathode, zinc foil anode, and glass wool separator, with 1.0 M $ZnSO_4$ aqueous electrolyte. The cells were galvanostatically cycled between 0.0 V and 1.5 V at the desired current rate using a MACCOR cycler. Cyclic voltammetry (CV) measurements were conducted at a scan rate of 0.03 mV s^{-1} using a VMP3 (Bio-Logic) potentiostat/galvanostat.

4. Material Characterization

The crystallographic structure of the synthesized materials was analyzed using powder X-ray diffraction (XRD). The patterns were obtained using an X-ray diffractometer (Bruker D8 Advanced LynxEye) with Cu-K_α radiation (λ=1.5405 Å). The morphology was observed using a field-emission scanning electron microscope (FE-SEM; FEI NOVA NanoSEM200). Chemical analysis of the synthesized materials was conducted using energy-dispersive X-ray spectroscopy (EDS) paired with FE-SEM (Hitachi S-4100). The local microstructure and compositional distribution of the cycled electrode were observed using high-resolution transmission electron microscopy (HR-TEM; Tecnai G2 F20, EFI).

RESULTS AND DISCUSSION

1. Structural and Morphological Characteristics of Reduced Lithium Titanate Spinel

The nano-crystallites of reduced lithium titanate spinel (r-LTO) were simply prepared by the thermochemical reduction of submicron LTO (200-300 nm) using a small amount of sodium borohydride ($NaBH_4$), at 400 °C, under argon atmosphere. This was accompanied by a distinct color change of LTO from white to dark blue or black, suggestive of bandgap narrowing through the introduction of oxygen vacancies; the color was well preserved for at least one year (Fig. 1(a), (b)). The X-ray diffraction (XRD) patterns

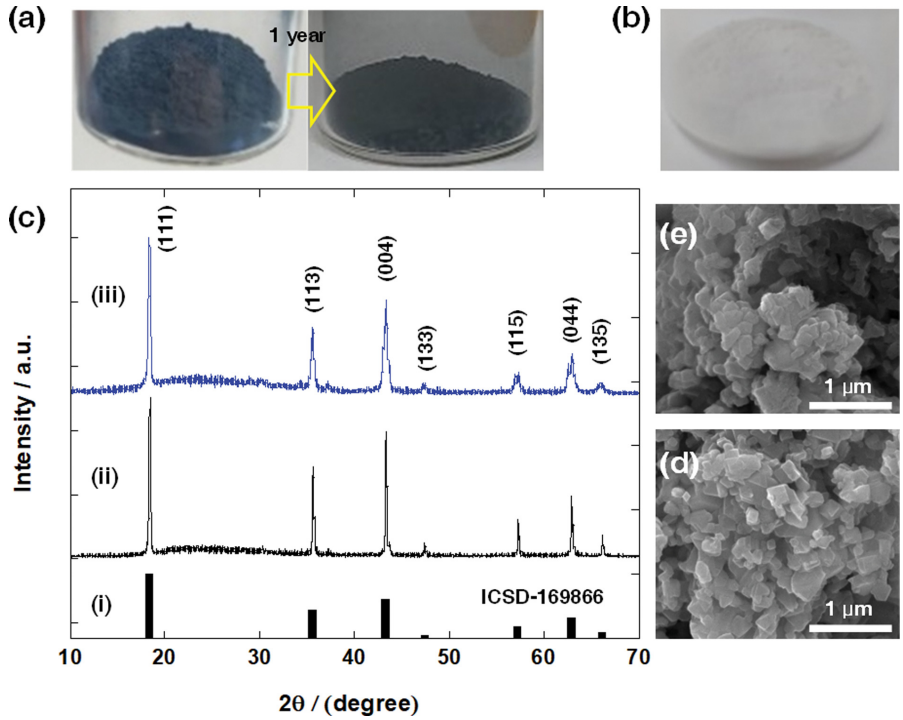

Fig. 1. Photographs of (a) as-prepared and one-year-old r-LTO powder (dark blue) and (b) pristine LTO (white). (c) XRD patterns of (i) reference LTO (stick pattern, ICSD-169866), (ii) LTO, and (iii) r-LTO. SEM images of (d) LTO and (e) r-LTO.

of r-LTO (Fig. 1(c)) can be indexed to a pure cubic spinel structure (Fd3-m), same with that of pristine LTO. However, the significant peak broadening in the pattern indicated that the crystallite domain was reduced to the nanoscale (~35 nm estimated from the Scherrer formula using the (111) reflection) after the thermochemical reduction. SEM observations of the sample morphology (Figs. 1(d), (e)) indicated that the overall particle size was maintained, but the much more rounded particle shape suggested that new small crystallites grew from the surface. More detailed morphological changes after the thermochemical reduction were observed through HR-TEM (Fig. 2). As opposed to pristine LTO with a smooth and ordered surface (Fig. 2(a), (b)), the surface of the r-LTO bulk particles was significantly amorphized (Fig. 2(d)) as a consequence of thermochemical reduction, and numerous fragments of the original particles (~30 nm) were attached to the surface (Fig. 2(c), Fig. S1), probably created and grown from the bulk particles. Compositional analysis by EDS indicated that r-LTO was almost Na-free (Fig. S2), indicating that redundant phases originating from the decomposition of reducing agent were effectively removed after washing with deionized water. The electrical conductivity of r-LTO, measured by the four-point probe method, was ~1.5×10^{-7} S cm^{-1}, which is many-orders higher than that of pristine LTO (~10^{-13} S cm^{-1} from the literature [32,33]). Previous studies have shown that reducing the particle size to nanoscale and increasing the electrical conductivity are effective strategies for enhancing the kinetics of Mg^{2+} integration into LTO [28-31]. This indicates that an efficient morphological and electronic structure for facile charge redistribution is essential for surmounting the large activation barrier posed by the increased coulombic interactions between the doubly charged intercalant ions (Mg^{2+}) and the host. Because Zn^{2+} is also doubly-charged with an ionic radius comparable to that of Mg^{2+}, a similar strategy may apply to Zn^{2+} insertion into LTO.

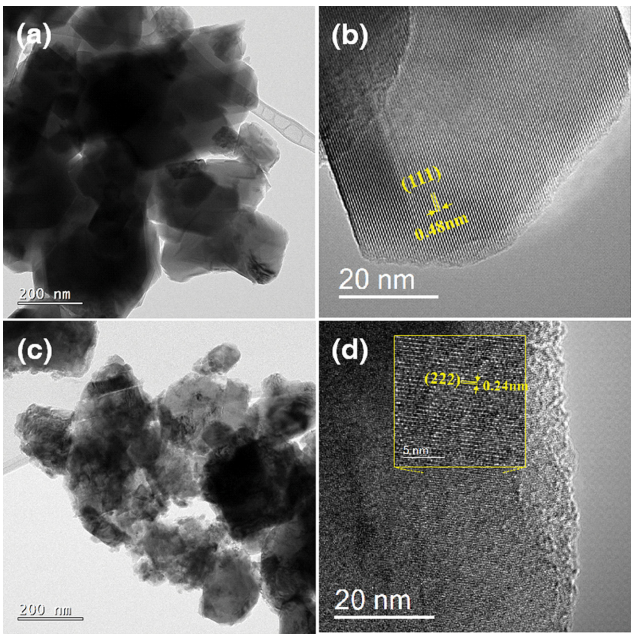

Fig. 2. HR-TEM images of (a), (b) LTO and (c), (d) r-LTO at low and high magnification. In (b) and (d), the lattice fringe spacings of 0.48 nm and 0.24 nm are consistent with the interplanar distance of the (111) planes of LTO and (222) planes in r-LTO, respectively.

2. Electrochemical behavior of r-LTO with Li^+ Ions

The electrochemical behavior of LTO upon integration of mon-

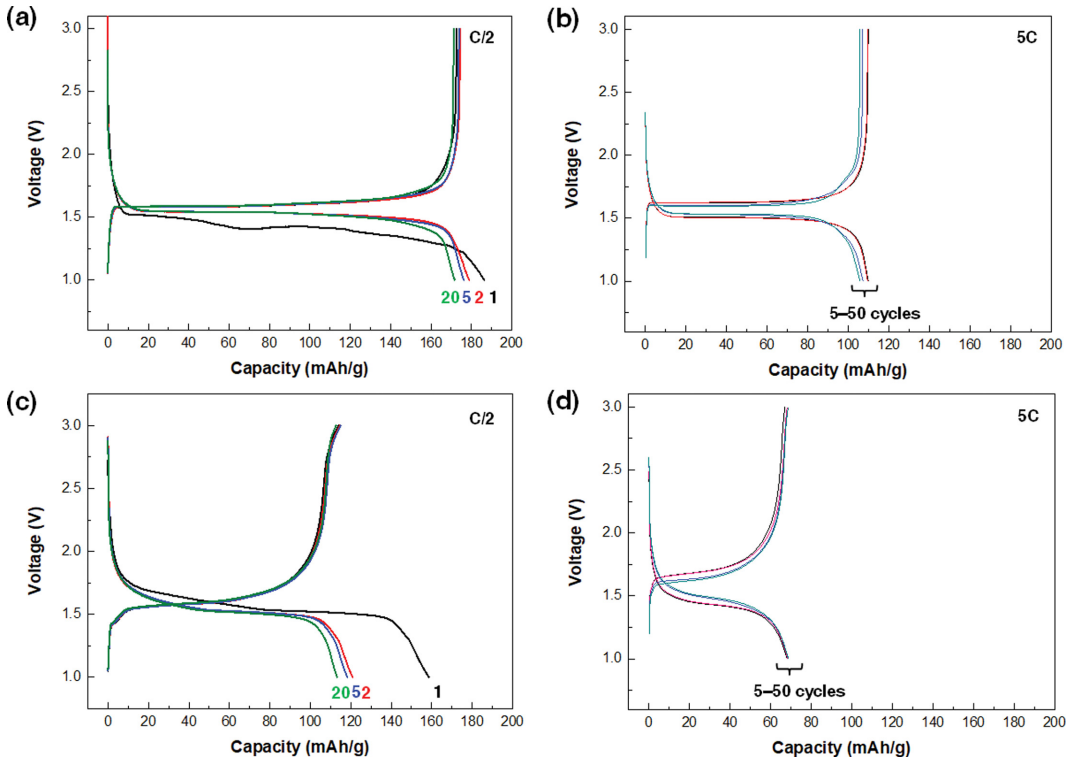

Fig. 3. Discharge-charge profiles of Li-ion battery cells with cathodes made of (a), (b) pristine LTO and (c), (d) r-LTO at a current rate of (a), (c) C/2 and (b), (d) 5C.

ovalent Li^+ was first evaluated by discharge-charge cycling at constant current rates (1C=175 mA g^{-1}) in the carbonate-based electrolytes. Pristine LTO showed a typical plateau potential at *ca.* 1.55 V for the two-phase reaction involving the formation of the lithiated phase, $Li_7Ti_5O_{12}$, delivering an almost theoretical capacity without significant fading for the extended cycling at C/2, while providing a reversible capacity of *ca.* 110 mAh g^{-1} at 5C (Fig. 3(a), (b)). In contrast, reduced LTO showed a sloping potential profile, and the capacity was decreased significantly to ~120 mAh g^{-1} at C/2 and 70 mAh g^{-1} at 5C (Fig. 3(c), (d)). The increased structural disorder and defects caused by thermochemical reduction may account for the significant decrease in the reversible capacity of r-LTO, as certain diffusion pathways for Li^+ possibly collapsed, and thus some redox sites were unavailable for Li^+ insertion. Furthermore, some intercalated Li^+ ions may have been trapped in the defect sites in r-LTO during the first discharge process, judging from the low coulombic efficiency (72%) in the first cycle (Fig. 3(c)). It is well known that the kinetics of ion insertion in LTO can be improved by reducing the particle size (or crystallite size) to the nanoscale, which shortens the diffusion pathway of the ions, enabling full utilization of the redox sites. Changing the electronic structure by aliovalent doping or introducing structural defects is another effective strategy, which facilitates the electron access to the reaction sites [28-31,34,35]. It was reported that the enhanced kinetics of nanosized particles may even lead to a fundamental change in the reaction mechanism, *e.g.*, from a two-phase reaction to a single-phase reaction, because the energy cost for forming new phase boundaries increases sharply as the particle size decreases to the nanoscale [36,37]. This may account for the sloping potential profile observed for r-LTO, which is a characteristic indicator of a single-phase reaction. Because particle (or crystallite) size reduction and good electrical conductivity are known as critical factors for the efficient intercalation of multivalent cations, r-LTO may exhibit better reaction kinetics for Zn^{2+} insertion than pristine LTO.

3. Electrochemical behavior of r-LTO with Zn^{2+} in Aqueous Electrolyte

The intercalation of Zn^{2+} ions into LTO and r-LTO was investigated in a 1.0 M $ZnSO_4$ aqueous electrolyte through galvanostatic cycling at a slow current rate of C/20 (Fig. 4(a)). The LTO spinel may be an attractive insertion host for Zn^{2+} because its large 3D tunnel was proven to be effective for the facile diffusion of Li^+ having an ionic radius similar to Zn^{2+} (0.74 Å/Zn^{2+} *vs.* 0.76 Å/Li^+). However, it was observed that pristine LTO exhibited low electrochemical activity with Zn^{2+}, delivering a discharge capacity of only 20 mAh g^{-1}, contrary to the case for Li^+ insertion. On the other hand, the reversible discharge capacity r-LTO was dramatically increased (~100 mAh g^{-1}), suggesting that the mechanism of divalent Zn^{2+} insertion was vastly different from that for monovalent Li^+. The increased capacity of r-LTO is possibly contributed by enhanced ion insertion kinetics originating from the reduced crystallite size and the increased electrical conductivity resulting from the thermochemical reduction. The large incipient discharge capacity (~230 mAh g^{-1}) and poor coulombic efficiency (22%) in the first cycle (Fig. 4(b)) might indicate that a significant amount of zinc ions was trapped in the structural defects in r-LTO owing to the greatly increased electrostatic interactions of Zn^{2+} with the r-LTO

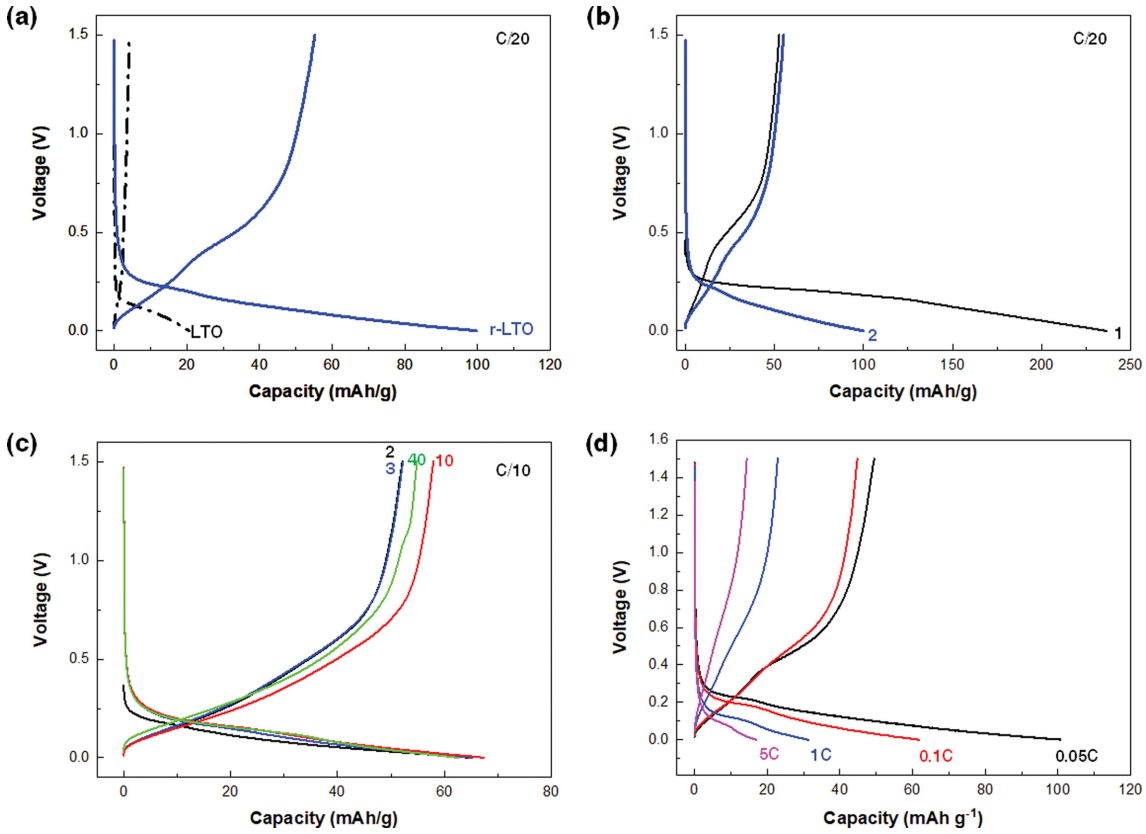

Fig. 4. (a) Comparison of typical discharge-charge profiles of Zn-ion battery cells with cathodes made of pristine LTO and r-LTO at C/20. (b) Comparison of discharge-charge profiles of cells with r-LTO cathode at the first and the second cycle at C/20. (c) Discharge-charge profiles of battery cells with r-LTO cathode at C/10 for 40 cycles. (d) Discharge-charge profiles of cells with r-LTO cathode at various current rates (C/20, C/10, 1C, 5C).

framework compared to Li^+, or substantial electrolyte decomposition, *e.g.*, hydrogen evolution reaction (HER), occurred on r-LTO, which might provide numerous catalytic surface defect sites. The average electrode potential for zinc insertion into r-LTO was estimated as ~0.2 V vs. Zn/Zn^{2+}, which is much lower than that of other potential candidate materials in the literature [17-20]. This is highly desirable for anode applications in terms of increasing overall energy density of battery considering the narrow stability window of the aqueous electrolytes. As shown in Fig. 4(c), r-LTO also afforded stable cycle performance at C/10 over 40 cycles, delivering a discharge capacity of ~65 mAh g^{-1}. The cyclic voltammogram for r-LTO (Fig. S3) shows multiple cathodic peaks ($E_{c,1}$, $E_{c,2}$) at *ca.* 0.05 and 0.15 V, with anodic peaks ($E_{a,1}$, $E_{a,2}$) at ~0.20 and ~0.50 V vs. Zn/Zn^{2+}, indicating that the insertion process might consist of a series of many reaction steps, as observed previously for Mg^{2+} intercalation into LTO [28-31]. The gradual shift of the redox peaks during cycling might indicate the slow development of stable ion-inserted or de-inserted LTO phases (*e.g.*, $Li_7Ti_5O_{12}$) during the initial electrochemical cycling [28-31]. Therefore, it is unlikely that the sloping potential observed for ion insertion into r-LTO in this study arises due to the single-phase reaction mechanism. The high activation barrier for multivalent cation diffusion through the solid framework (~0.8 eV for Mg^{2+}) and the energy cost associated with the de-solvation of Zn^{2+} at the interface are other factors to consider that may impede the facile single-phase reaction route [31]. The complicated reaction steps may involve the migration of both Li^+ and Zn^{2+} between the adjacent LTO phases and the participation of more than two reaction phases, similar to the case for Mg^{2+} insertion into LTO nano-particles, which could lead to sloping potential profiles [28-31]. Fig. 4(d) shows the performance at various current rates. r-LTO delivered a reversible capacity of over 30 mAh g^{-1} even at a high current rate of 1C, in contrast with pristine LTO, which afforded almost negligible capacity at the same current rate. These results indicate that r-LTO can be utilized as an insertion host for anode materials in zinc-ion batteries.

DISCUSSION

To investigate the reaction mechanism of r-LTO with Zn^{2+}, fully discharged and recharged r-LTO electrodes were prepared and their XRD patterns were measured (Fig. 5). Both patterns show the presence of two main reaction products: r-LTO and zinc hydroxide sulfate hydrate ($Zn_4(OH)_6SO_4{\cdot}zH_2O$, ZHS). ZHS is a commonly observed reaction product in cycled electrodes in zinc-ion batteries employing $ZnSO_4$ electrolytes, where z ranges from 0 to 5 [38-40]. The formation of ZHS is usually induced by an increase in the pH of the electrolyte owing to various causes [40]. In the present case, the parasitic zinc corrosion reaction on the counter elec-

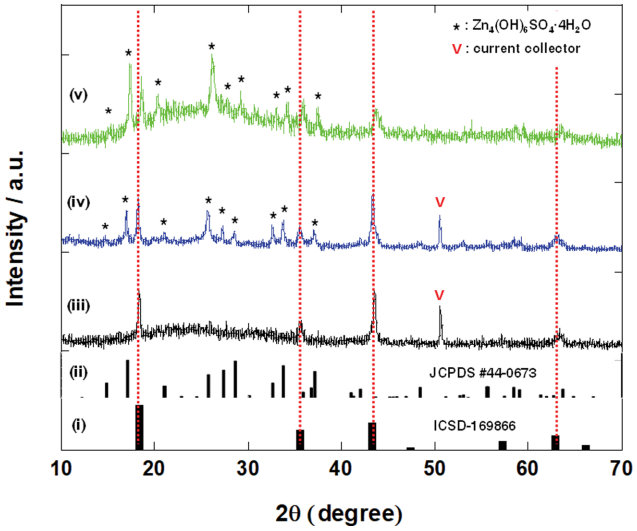

Fig. 5. XRD patterns of (i) reference LTO (stick pattern, ICSD-169866), (ii) reference ZHS ($Zn_4(OH)_6SO_4{\cdot}4H_2O$) (stick pattern, JCPDS #44-0673), (iii) as-prepared electrode, (iii) fully discharged r-LTO electrode, and (iv) fully recharged r-LTO electrode. The cycled electrodes were prepared from the zinc-ion battery cells.

trode ($Zn+2H^+ \rightarrow Zn^{2+}+H_2(g)$) is probably responsible for the formation of ZHS, as the continued hydrogen evolution reaction might increase the pH of the electrolyte. It is noteworthy that the formation of ZHS on the cathode may enhance the ion insertion kinetics. It was reported that ZHS on Mo_6S_8 could regenerate the hydroxylated surface of Mo_6S_8, promoting free and unimpeded adsorption of zinc ion complexes on the surface. This can lower the energy cost associated with desolvation of zinc ions, enhancing the insertion kinetics [19]. ZHS precipitation on r-LTO might induce similar effect to promote Zn^{2+} insertion. The slightly increased relative intensity of ZHS in the fully recharged electrode compared to that of the fully discharged electrode indicates that the amount of ZHS increased with time as zinc corrosion continued. There was almost no change in the position of the XRD peaks for the zinc-inserted r-LTO phase from the fully-discharged electrode as well as zinc-extracted r-LTO phase from the fully-recharged electrode (Fig. 5(iv), (v)) compared to that of uncycled r-LTO, reflecting the 'zero strain' character. Furthermore, the Zn content of r-LTO in the fully discharged electrode was confirmed by EDS elemental mapping (Fig. 6), which showed that the distribution of Zn agreed well with those of Ti and O. The ratio of Zn to Ti was estimated to be around 0.07 corresponding to the capacity of about 40 mAh g^{-1}, while the initial discharge capacity was measured over 200 mAh g^{-1} (Fig. 4(b)). This might indicate that electrolyte decomposition reaction was one of main contributors to the low Coulombic efficiency at the first cycle as discussed earlier.

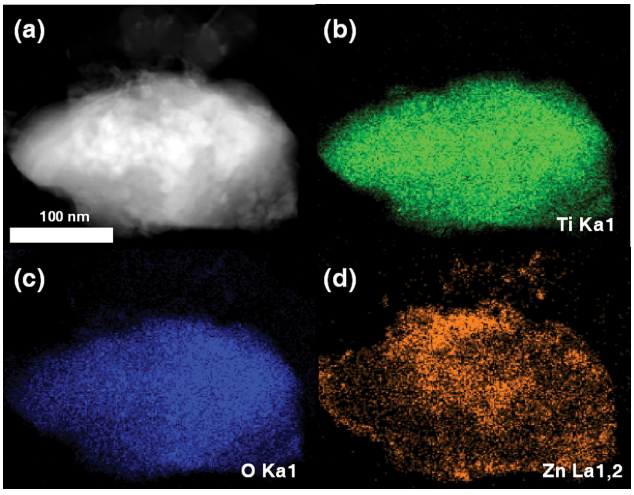

Fig. 6. Relative distribution of chemical elements in a single r-LTO particle from the fully discharged electrode of zinc-ion battery cell. (a) TEM image and EDS maps of individual elements including (b) Ti, (c) O, and (d) Zn.

CONCLUSIONS

Reduced LTO was prepared via a simple thermochemical reduction process at 400 °C with $NaBH_4$ as a reducing agent, and was investigated for the first time as a plausible insertion host for zinc ion battery anodes. We demonstrated that thermochemical reduction of LTO led to a significant reduction in the particle size and drastic enhancement in the electrical conductivity, which contributed critically to improving the ion insertion kinetics and increasing the reversible capacity. Structural and morphological studies confirmed that r-LTO serves as a zero-strain host for Zn^{2+} insertion, *albeit* it reduces Coulombic efficiency at the first cycle. Electrochemical investigation showed that r-LTO exhibits an electrode potential of *ca.* 0.2 V, which is highly desirable for anode materials, delivering a discharge capacity of ~100 mAh g^{-1} at C/20 and stable cycle performance for the extended cycles. This study provides a promising strategy for unearthing new intercalation hosts for constructing rechargeable batteries based on earth-abundant multivalent metal cations.

ACKNOWLEDGEMENTS

This work was financially supported by the National Research Foundation of Korea (NRF) (NRF-2021R1A2C2008680 and NRF-2017R1A6A1A06015181).

SUPPORTING INFORMATION

Additional information as noted in the text. This information is available via the Internet at http://www.springer.com/chemistry/journal/11814.

REFERENCES

1. D. Selvakumaran, A. Pan, S. Liang and G. Cao, *J. Mater. Chem. A*, **7**, 18209 (2019).
2. M. Song, H. Tan, D. Chao and H. J. Fan, *Adv. Funct. Mater.*, **28**, 1802564 (2018).
3. M. Mao, T. Gao, S. Hou and C. Wang, *Chem. Soc. Rev.*, **47**, 8804 (2018).

4. R. Mohtadi and F. Mizuno, *Beilstein J. Nanotechnol.*, **5**, 1291 (2014).
5. H. Yang, H. Li, J. Li, Z. Sun, K. He, H.-M. Cheng and F. Li, *Angew. Chem. Int. Ed.*, **58** 11978 (2019).
6. C. Xu, B. Li, H. Du and F. Kang, *Angew. Chem. Int. Ed.*, **51**, 933 (2012).
7. S. Huang, J. Zhu, J. Tian and Z. Niu, *Chem. Eur. J.*, **25**, 14480 (2019).
8. J. Shin, J. Lee, Y. Par and J. W. Choi, *Chem. Sci.*, **11** 2028 (2020).
9. S. Gürmen and M. Emre, *Miner. Eng.*, **16**, 559 (2003).
10. Z. Liu, Y. Huang, Y. Huang, Q. Yang, X. Li, Z. Huang and C. Zhi, *Chem. Soc. Rev.*, **49**, 180 (2020).
11. W. Lu, C. Xie, H. Zhang and X. Li, *ChemSusChem*, **11**, 3996 (2018).
12. T. Zhang, Y. Tang, S. Guo, X. Cao, A. Pan, G. Fang, J. Zhou and S. Liang, *Energy Environ. Sci.*, **13**, 4625 (2020).
13. X. Xie, S. Liang, J. Gao, S. Guo, J. Guo, C. Wang, G. Xu, X. Wu, G. Chen and J. Zhou, *Energy Environ. Sci.*, **13**, 503 (2020).
14. K. Zhao, C. Wang, Y. Yu, M. Yan, Q. Wei, P. He, Y. Dong, Z. Zhang, X. Wang and L. Mai, *Adv. Mater. Interfaces*, **5**, 1800848 (2018).
15. K. E. K. Sun, T. K. A. Hoang, T. N. L. Doan, Y. Yu, X. Zhu, Y. Tian and P. Chen, *ACS Appl. Mater. Interfaces*, **9**, 9681 (2017).
16. K. Wipermann, J. W. Schultze, R. Kessel and J. Penninger, *Corros. Sci.*, **32**, 205 (1991).
17. Y. Cheng, L. Luo, L. Zhong, J. Chen, B. Li, W. Wang, S. X. Mao, C. Wang, V. L. Sprenkle, G. Li and J. Liu, *ACS Appl. Mater. Interfaces*, **8**, 13673 (2016).
18. M. S. Chae, J. W. Heo, S.-C. Lim and S.-T. Hong, *Inorg. Chem.*, **55**, 3294 (2016).
19. B. Lee, W. J. No and S. H. Oh, *J. Power Sources*, **478**, 229086 (2020).
20. L. Yan, X. Zeng, Z. Li, X. Meng, D. Wei, T. Liu, M. Ling, Z. Lin and C. Liang, *Mater. Today Energy*, **12**, 323 (2019).
21. L. Chen, J. L. Bao, X. Dong, D. G. Truhlar, Y. Wang, C. Wang and Y. Xia, *ACS Energy Lett.*, **2**, 1115 (2017).
22. D. Aurbach, Z. Lu, A. Schechter, Y. Gofer, H. Gizbar, R. Turgeman, Y. Cohen, M. Moshkovich and E. Levi, *Nature*, **407**, 724 (2000).
23. D.-M. Kim, S. C. Jing, S. Ha, Y. Kim, Y. Park, J. H. Ryu, Y.-K. Han and K. T. Lee, *Chem. Mater.*, **30**, 3199 (2018).
24. L. Zhou, Q. Liu, Z. Zhang, K. Zhang, F. Xiong, S. Tan, Q. An, Y.-M. Kang, Z. Zhou and L. Mai, *Adv. Mater.*, **30**, 1801984 (2018).
25. L. Aldon, P. Kubiak, M. Womes, J. C. Jumas, J. Olivier-Fourcade, J. L. Tirado, J. I. Corredor and C. P. Vicente, *Chem. Mater.*, **16**, 5721 (2004).
26. K.-S. Park, A. Benayad, D.-J. Kang and S.-G. Doo, *J. Am. Chem. Soc.*, **130**, 14930 (2008).
27. Y.-Q. Wang, L. Gu, Y.-G. Guo, H. Li, X.-Q. He, S. Tsukimoto, Y. Ikuhara and L.-J. Wan, *J. Am. Chem. Soc.*, **134**, 7874 (2012).
28. N. Wu, Y. X. Yin and Y. G. Guo, *Chem-Asian J.*, **9**, 2099 (2014).
29. N. Wu, Y.-C. Lyu, R.-J. Xiao, X. Yu, Y.-X. Yin, X.-Q. Yang, H. Li, L. Gu and Y.-G. Guo, *NPG Asia Mater.*, **6**, e120 (2014).
30. N. Wu, Z. Z. Yang, H. R. Yao, Y. X. Yin, L. Gu and Y. G. Guo, *Angew. Chem. Int. Ed.*, **54**, 5757 (2015).
31. B. Lee, E. Jo, J. Choi, J. H. Kim, W. Chang, S. Yu, H.-S. Kim and S. H. Oh, *J. Mater. Chem. A*, **44**, 25619 (2019).
32. H. Song, S. W. Yun, H. H. Chun, M. G. Kim, K. Y. Chung, H. S. Kim, B. W. Cho and Y. T. Kim, *Energy Environ. Sci.*, **5**, 9903 (2012).
33. T. F. Yi, S. Y. Yang and Y. Xie, *J. Mater. Chem. A*, **3**, 5750 (2015).
34. Y. Wang, H. Li, P. He, E. Hosono and H. Zhou, *Nanoscale*, **2**, 1294 (2010).
35. J. Lu, Z. Chen, Z. Ma, F. Pan, L. A. Curtiss and K. Amine, *Nat. Nanotechnol.*, **11**, 1031 (2016).
36. M. Wagemaker, W. J. H. Borghols and F. M. Mulder, *J. Am. Chem. Soc.*, **129**, 4323 (2007).
37. N. Meethong, H.-Y. S. Huang, W. C. Carter and Y.-M. Chiang, *Electrochem. Solid-State Lett.*, **10**, A134 (2007).
38. S. Zhao, B. Han, D. Zhang, Q. Huang, L. Xiao, L. Chen, D. G. Ivey, Y. Deng and W. Wei, *J. Mater. Chem. A*, **6**, 5733 (2018).
39. A. Moezzi, M. B. Cortie and A. M. McDonagh, *Dalton Trans.*, **42**, 14432 (2013).
40. B. Lee, H. R. Seo, H. R. Lee, C. S. Yoon, J. H. Kim, K. Y. Chung, B. W. Cho and S. H. Oh, *ChemSusChem*, **9**, 2948 (2016).

Supporting Information

Investigation of reduced lithium titanate spinel as insertion host for rechargeable batteries

Minji Jeong[*,,‡], Min Jin Kim[*,‡], Subin Na[*], Seulki Han[*], Eunmi Jo[*], Seung-Ho Yu[**], Taeeun Yim[***,†], and Si Hyoung Oh[*,****,†]**

*Energy Storage Research Center, Korea Institute of Science and Technology,
5, Hwarang-ro 14-gil, Seongbuk-gu, Seoul 02792, Korea
**Department of Chemical and Biological Engineering, Korea University, 145, Anam-ro, Seongbuk-gu, Seoul 02841, Korea
***Department of Chemistry, Research Institute of Basic Sciences, College of Natural Science,
Incheon National University, 119 Academy-ro, Yeonsu-gu, Incheon 22012, Korea
****Division of Energy & Environment Technology, Korea University of Science and Technology, Seoul 02792, Korea
(*Received 16 August 2022 • Revised 24 October 2022 • Accepted 6 November 2022*)

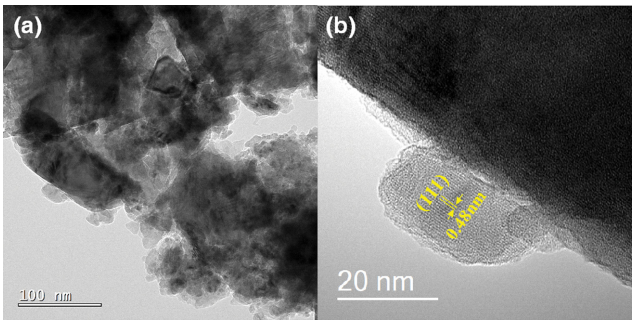

Fig. S1. HR-TEM images of r-LTO in (a) low and (b) high magnifications. In r-LTO, numbers of nano-sized particles were attached on the bulk particles. In (b), lattice fringe spacing of 0.48 nm was consistent with the interplanar distance of (111) planes of r-LTO, indicating that nano particles were r-LTO created during the thermochemical reduction.

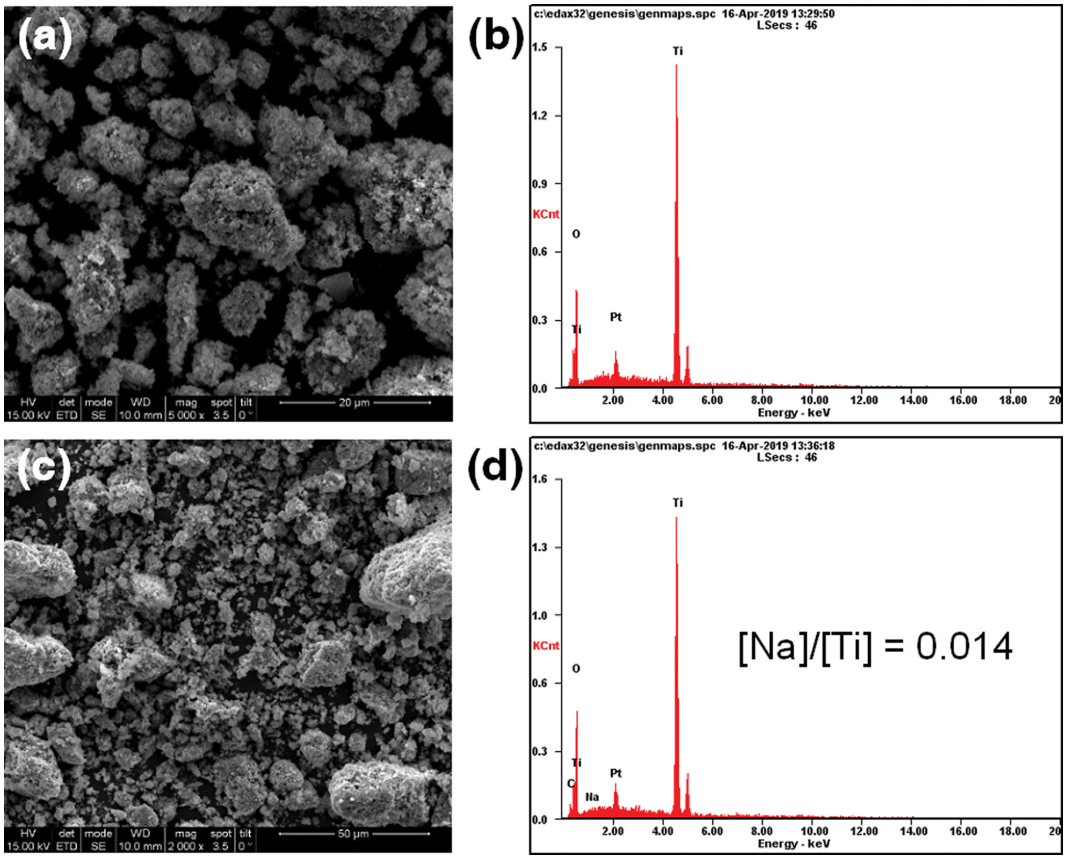

Fig. S2. SEM images and corresponding EDS elemental analysis of (a), (b) pristine LTO and (c), (d) r-LTO, respectively. Peak for Na Kα (at 1.041 keV) was not detected clearly either in pristine LTO or r-LTO. [Na]/[Ti] ratio in r-LTO was found to be 0.014, indicating that Na content in r-LTO was negligible.

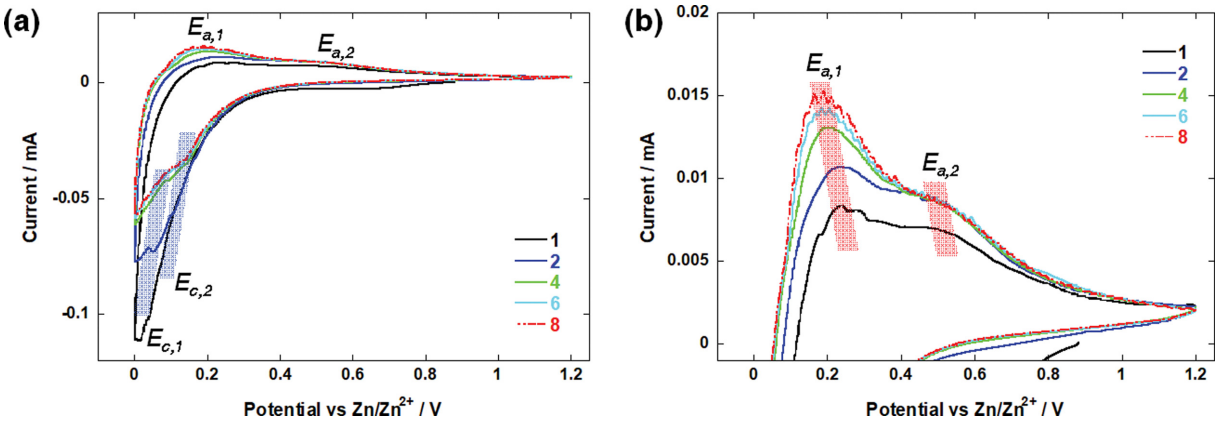

Fig. S3. (a) Cyclic voltammograms for r-LTO at a scan rate of 0.03 mV s^{-1} and (b) enlarged graphs for anodic peaks. After the initial activation that had lasted a few cycles, the profiles were fully developed showing multiple redox peaks, *i.e.*, $E_{c,1}$, $E_{c,2}$ and $E_{a,1}$, $E_{a,2}$ for cathodic and anodic process, respectively. This probably indicated that zinc intercalation occurred via a complicated reaction mechanism involved with both Li^+ and Zn^{2+} migration between the adjacent phases similar to Mg^{2+} insertion into LTO nano particles.